

Synthesis, characterization and in silico evaluation of 2,5-bis(2-(trifluoromethyl)-1H-benzimidazol-5-yl)-1,3,4-oxadiazole: Reactivity, ADME/toxicity, and docking against therapeutic targets

Assiya Atif^{a*}, Soukaina Ameur^{a,b} and Houssine Ait Sir^a

^aBioorganic Chemistry Team, Laboratory of Bioorganic Chemistry, Faculty of Sciences, Chouaib Doukkali University, 24000 El Jadida, Morocco

^bMolecular Modeling and Spectroscopy Research Team, Faculty of Sciences, Chouaib Doukkali University, 24000 El Jadida, Morocco

CHRONICLE

Article history:

Received March 15, 2025

Received in revised form

June 9, 2025

Accepted August 9, 2025

Available online

August 9, 2025

Keywords:

Synthesis

Characterization

1,3,4-oxadiazole

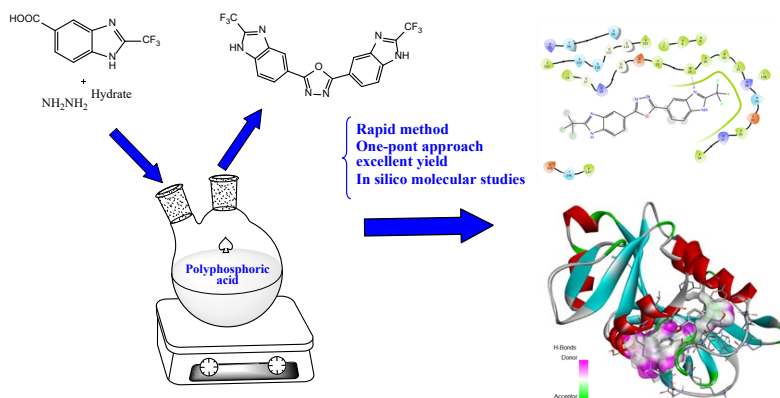
Reactivity

Docking

ABSTRACT

This study presents the synthesis and characterization of a novel 1,3,4-oxadiazole derivative compound, 2,5-bis(2-(trifluoromethyl)-1H-benzimidazol-5-yl)-1,3,4-oxadiazole, using ¹H NMR, ¹³C NMR, mass spectrometry and FTIR-ATR infrared spectroscopy. Reactivity, ADME/toxicity and docking to therapeutic targets were investigated revealed that 2,5-bis(2-(trifluoromethyl)-1H-benzimidazol-5-yl)-1,3,4-oxadiazole (BTBO) exhibits excellent intestinal absorption, limited solubility and CNS penetration, and retained clearance. It interacts with key cytochromes and transporters, suggesting possible drug–drug interactions. Toxicity evaluations indicated mutagenic potential and moderate oral toxicity, with no hepatotoxicity or skin sensitization. Molecular docking demonstrated strong binding affinities to targets in six therapeutic areas, often outshining reference ligands, supporting its auspicious pharmacokinetic and therapeutic potential.

© 2025 by the authors; licensee Growing Science, Canada.



Graphical representation

1. Introduction

Heterocyclic compounds are cyclic organic compounds that contain at least one heteroatom. Nitrogen, oxygen, and sulfur are the most commonly encountered, but there are also many heterocyclic rings containing other heteroatoms. Heterocyclic compounds are considered as one of the essential classes of organic compounds, used in a multitude of biological fields due to their involvement in various conditions¹. Oxadiazoles, five-membered heterocycles consisting of two carbon atoms, two

* Corresponding author

E-mail address assis.atif@gmail.com (A. Atif)

nitrogen atoms, and a single oxygen atom, are attracting major attention in various fields of medicinal chemistry and pesticides, but also in polymer and materials science². Oxadiazole rings can exist in different regioisomeric forms³.

There are several compounds containing 1,3,4-oxadiazole available commercially, such as, raltegravir is a human immunodeficiency virus (HIV) integrase inhibitor, active against HIV-1⁴, the emergence of resistance is certainly faster than for protease inhibitors/ritonavir. Several factors could be involved in resistance to raltegravir, such as viral load level and replication time, genetic polymorphism of the virus (integrase gene and other genes, viral subtype), as well as plasma and/or intracellular concentration of raltegravir. Furamizol has antibacterial activity⁵, studies on the in vitro sensitivity of mycoplasmas isolated from various animals to heterocycles indicate that furamizol has an inhibitory effect at concentrations below 0.5 µg/ml and zibotentan is an experimental anti-cancer⁶, zibotentan is a specific ETA receptor antagonist in clinical development for the treatment of hormone-refractory prostate cancer (HRPC). In preclinical studies, zibotentan inhibited ET-1-induced changes in cell invasiveness in vitro, as well as angiogenesis, metastasis, and tumor xenograft growth in vivo. Consistent with its specific binding profile, zibotentan inhibited ETA receptor-mediated antiapoptotic events, while allowing ETB receptor-mediated proapoptotic signaling (**Fig 1**).

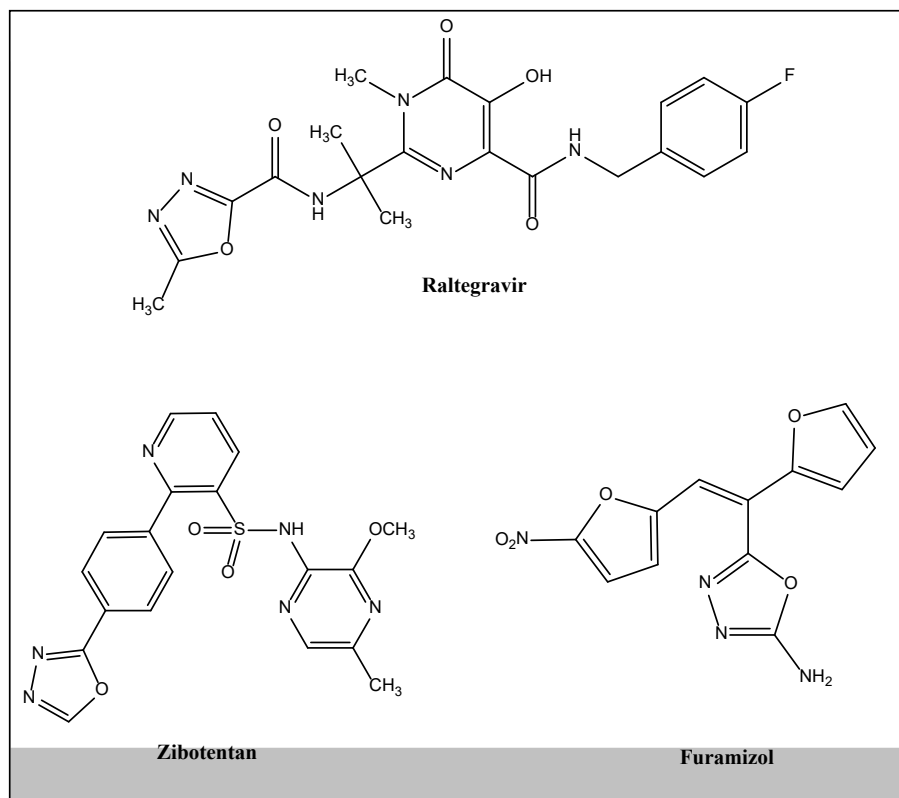


Fig 1. Structure of Raltegravir, Zibotentan and Furamizol.

1,3,4-Oxadiazole has found many pharmaceutical applications. For several years, researchers have been manufacturing new compounds containing the 1,3,4-oxadiazole core, demonstrating a broad spectrum of biological activity, in particular anti-inflammatory⁷⁻¹⁰, analgesic¹¹, anti-depressive¹²⁻¹³, anticancer¹⁴⁻¹⁵, anti-diabetic¹⁶⁻¹⁷, effect, antibacterial¹⁸⁻²⁰, antifungal²¹⁻²² and antiviral²³⁻²⁴.

Building on this growing body of research, our study emphasizes synthesis, characterization of a novel 1,3,4-oxadiazole derivative compound, 2,5-bis(2-(trifluoromethyl)-1H-benzimidazol-5-yl)-1,3,4-oxadiazole, using ¹H NMR, ¹³C NMR, mass spectrometry, FTIR-ATR infrared spectroscopy and computational inquiry, which combines the 1,3,4-oxadiazole main with benzimidazole and fluorinated groups components that are known to increase pharmacological activity. The target of this study was to explore its electronic properties, reactivity, and potential therapeutic applications across computational simulations.

To explore the compound's reactivity, we performed theoretical calculations to identify its electronic structure. This included an analysis of its boundary molecular orbitals (HOMO and LUMO)²⁵ and the Molecular Electrostatic Potential (MEP)²⁶ to identify the electrophilic and nucleophilic areas of the molecule. Moreover, we carried out ADME²⁷ (Absorption, Distribution, Metabolism, and Excretion) and toxicity predictions to value its pharmacokinetic properties and toxicity potential, providing insights into its drug-like characteristics. Likewise, molecular docking²⁸ studies were conducted to assess the compound's binding affinity toward various biological targets involved in key therapeutic areas such as anticancer, antibacterial, antifungal, anti-inflammatory, antioxidant, and antitubercular activities.

2. Materials and Methods

2.1. Reagents and instruments

All reagents and solvents used in this study were purchased from Sigma-Aldrich and employed without further purification. Reaction progress was monitored by thin-layer chromatography (TLC) using aluminum plates coated with Merck 60 F254 silica gel (thickness: 0.2 mm), with visualization under UV light at 254 and 365 nm. Melting points of the synthesized compounds were determined using a Köfler bench and are uncorrected. FT-IR spectra were recorded using a SHIMADZU FT-IR 8400S spectrometer equipped with a Smart iTR accessory and a diamond ATR crystal, over the range of 500–4000 cm^{-1} . NMR analyses (^1H at 500 MHz and ^{13}C at 125 MHz) were performed on a JEOL JNM-ECZ500/S1 FT-NMR system at the National Center for Scientific and Technical Research (CNRST) in Rabat, with chemical shifts referenced to the solvent used (DMSO-d_6 : ^1H and ^{13}C). The description of materials and analytical procedures was partially inspired by methods reported in a previous study²⁹.

2.2. Calculation methodology

To evaluate 2,5-bis(2-(trifluoromethyl)-1H-benzo[d]imidazol-5-yl)-1,3,4-oxadiazole reactivity and its biological interaction potential, an *in silico* study³⁰ was performed, combining quantum chemical calculations and molecular docking simulations³¹. Initially, the molecular structure was optimized using Density Functional Theory (DFT) at the B3LYP/6-311G(d,p) level of theory. This level was selected based on its proven reliability in the study of structurally related heterocyclic compounds, particularly azoles and oxadiazoles, as demonstrated in recent studies^{32,33}. Following geometry optimization, the frontier molecular orbitals (HOMO and LUMO) and Molecular Electrostatic Potential (MEP) were calculated to gain visions into the electronic distribution and the reactive sites of the molecule³⁴. Parallel, molecular docking studies were carried out to calculate the compound's binding affinity to a range of biological targets connected with key therapeutic areas: anticancer, antibacterial, antifungal, anti-inflammatory, antioxidant, and antitubercular. The docking simulations were performed using AutoDock Tools and AutoDock Vina, with the binding interactions visualized through Maestro (Schrödinger). The three-dimensional structures of the target proteins were acquired from the Protein Data Bank (PDB)³⁵, and reference ligands were sourced from PubChem³⁶ for contrast and performance evaluation.

2.3. Synthesis

2.3.1. Synthesis of 2-(trifluoromethyl)-1H-benzimidazole-5-carboxylic acid (3)

To a solution of 3,4-diaminobenzoic acid (**1**) (40 mmol) in concentrated hydrochloric acid (30 ml) was added 2,2,2-trifluoroacetic acid (**2**) (60 mmol). The reaction mixture was refluxed for 6 hours. After cooling, the reaction medium was brought to pH = 4 with 25% ammoniac, the precipitate formed was filtered and recrystallized from ethanol³⁷. Yield 92%, beige powder, m.p > 300°C. IR spectrum, ν , cm^{-1} : 3256 (N-H), 2967-3085 (O-H), 1746 (C=O), 1632 (C=N), 1010 (C-F). ^1H NMR spectrum, δ , ppm: 7.56(d,1H,CHar), 7.75(s,1H,CHar), 8.04(d,1H,CHar), 11.07(s,1H,NH), 11.24(s,1H,OH). ^{13}C NMR spectrum, δ , ppm: 168.10(C=O), 148.35(Car), 146.80(C=N), 136.44(Car), 124.53(Car), 124.14(Car), 120.80(Car), 120.66(C-F), 115.21(Car). Mass spectrum, m/z: 231 [M+H]⁺ (90).

2.3.2. Synthesis of 2,5-bis(2-(trifluoromethyl)-1H-benzimidazol-5-yl)-1,3,4-oxadiazole (4)

This synthesis consists of fusing two equivalents of a derivative of 2-(trifluoromethyl)-1H-benzimidazole-5-carboxylic acid (**3**) with one equivalent of hydrazine hydrate in polyphosphoric acid (5 ml) at reflux for 4 hours. At the end of the reaction, the mixture is neutralized with sodium hydroxide NaOH to pH = 7, the solid formed is filtered, washed and recrystallized from ethanol³⁸. Yield 86%, brown powder, m.p > 300°C. IR spectrum, ν , cm^{-1} : 3086 (N-H), 1625 (C=N), 1029 (C-F). ^1H NMR spectrum, δ , ppm: 7.46(d,2H,CHar), 7.70(s,2H,CHar), 7.99(d,2H,CH), 10.64(s,2H,NH). ^{13}C NMR spectrum, δ , ppm: 162.86(2C=N), 147.24(2C=N), 135.52(2Car), 134.41(2Car), 130.08(2Car), 124.14(2Car), 120.69(2C-F), 115.51(2Car), 114.79(2Car). Mass spectrum, m/z: 439 [M+H]⁺ (97).

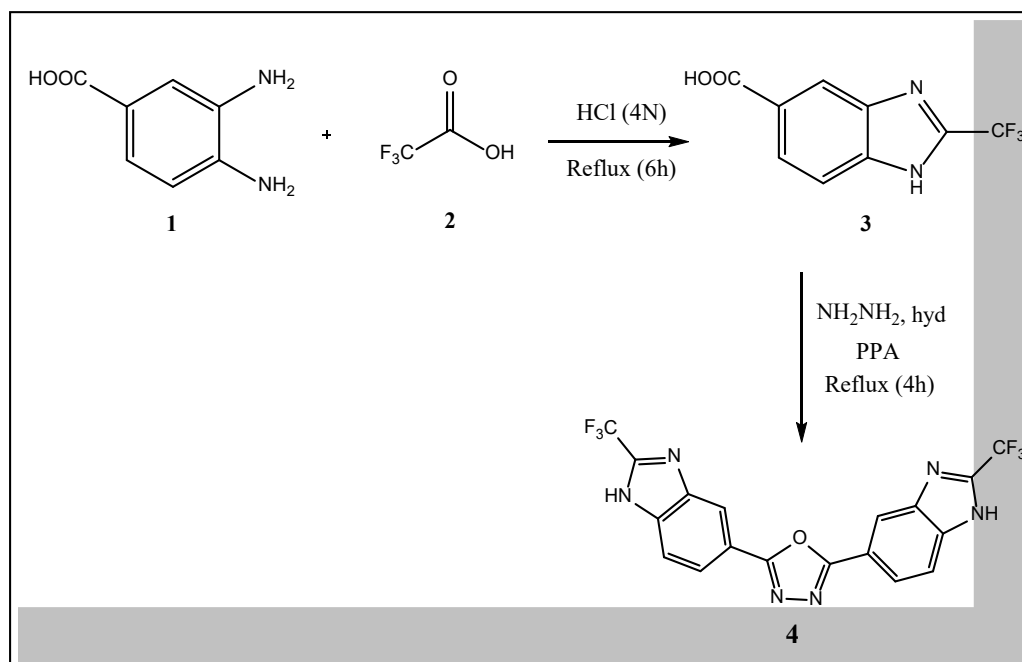
3. Results and Discussion

3.1. Synthesis of 2,5-bis(2-(trifluoromethyl)-1H-benzimidazol-5-yl)-1,3,4-oxadiazole

Many methods for the synthesis of symmetrical 1,3,4-oxadiazole derivatives have been reported in the literature^{39,40}, the advantage of this type of reaction is that it takes place in a single step from a carboxylic acid derivative, which is very advantageous in terms of cost.

On our part, 2-(Trifluoromethyl)-1H-benzimidazole-5-carboxylic acid (**3**) was prepared in good yield^{41,42} by the condensation of 3,4-diaminobenzoic acid (**1**) (OPDA) with acetic acid in hydrochloric acid according to the method of Phillips^{43,44}. Then, we proceeded to the synthesis of 2,5-bis(2-(trifluoromethyl)-1H-benzimidazol-5-yl)-1,3,4-oxadiazole (**4**)

by reacting two equivalents of 2-(trifluoromethyl)-1H-benzimidazole-5-carboxylic acid (**3**) with one equivalent of hydrazine hydrate in 5 ml of polyphosphoric acid at reflux for 4 hours. After treatment, the precipitate obtained is then recrystallized from ethanol³⁸. The compound (**4**) is obtained with a yield of 86% and a melting temperature greater than 300°C. (**Scheme 1**)



Scheme 1. Synthesis of 2,5-bis(2-(trifluoromethyl)-1H-benzimidazol-5-yl)-1,3,4-oxadiazole

The structure of Spectral analysis of 2,5-bis(2-(trifluoromethyl)-1H-benzimidazol-5-yl)-1,3,4-oxadiazole was characterized and confirmed using IR, ¹H NMR, ¹³C NMR and MS.

The IR spectrum reveals an absorption band at 1625 cm⁻¹ due to the presence of a C=N bond, a band at 3086 cm⁻¹ corresponding to N-H and a band at 1029 cm⁻¹ for C-F.

On the ¹H NMR spectrum, we observe the appearance of a singlet at 10.64 ppm attributable to the benzimidazole proton and the masses between 7.46 and 7.99 ppm corresponding to the aromatic protons.

The analysis of the ¹³C NMR spectrum corroborates this confirmation. Indeed, it clearly highlights the presence of three signals at 162.86 and 147.24 ppm of the C=N bonds and signals at 135.52, 134.41, 130.08, 124.14, 120.69, 115.51 and 114.79 ppm due to the cyclic carbons.

The mass spectrum, taken in (ESI), shows a molecular peak relative to the molecular ion $m/z = 439[M+H]^+$.

3.2. Analysis of overall reactivity indexes

To determine the electrophilic and nucleophilic properties of the compound 2,5-bis(2-(trifluoromethyl)-1H-benzo[d]imidazol-5-yl)-1,3,4-oxadiazole, HOMO and LUMO energies were calculated (**Table 1**). The results show a chemical potential of -4.198 eV, indicating moderate electron-accepting ability. The chemical hardness of 4.373 eV suggests high electronic stability. The compound displays moderate electrophilicity (2.015 eV) and good nucleophilicity (2.984 eV), revealing a balanced reactivity profile. These properties make it a promising candidate for molecular interactions in biological systems.

Table 1. Electronic chemical potential (μ), chemical hardness (η), electrophilicity (ω), and nucleophilicity index (N) of 2,5-bis(2-(trifluoromethyl)-1H-benzo[d]imidazol-5-yl)-1,3,4-oxadiazole.

System	HOMO (u.a)	LUMO (u.a)	N (eV)	ω (eV)	μ (eV)	η (eV)
Product	-0.23464	-0.07394	2.98	2.01	-4.19	4.37

Molecular electrostatic potential (MEP) analysis identifies the regions of a molecule likely to be involved in electrostatic interactions, highlighting areas rich or poor in electron density. The MEP surface of our optimized compound has been calculated at the DFT/B3LYP/6-311G (d,p) level and is illustrated in the **Fig. 2**.

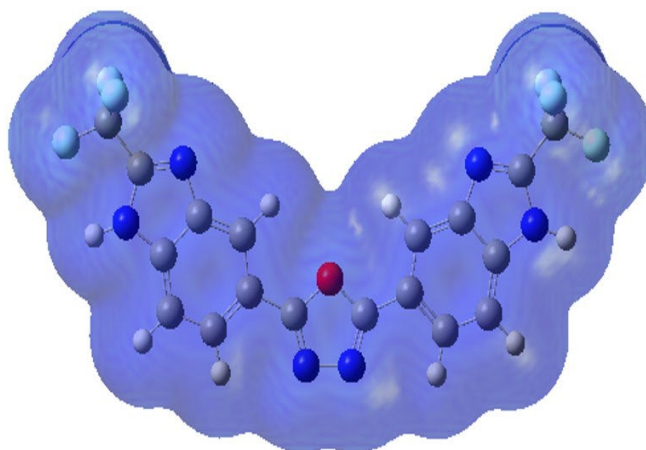


Fig. 2. 3D-MEPs for the title (3d) compound: 2,5-bis(2-(trifluoromethyl)-1H-benzo[d]imidazol-5-yl)-1,3,4-oxadiazole

The resulting MEP map shows predominant blue coloration across the molecular surface, indicating low overall electrostatic polarization. Potential values range from around -4.061×10^{-4} to 4.061×10^{-4} a.u., reflecting a low contrast in electrostatic potential. This suggests that the molecule does not contain distinctly strong electrophilic or nucleophilic centers, but instead exhibits a relatively homogeneous distribution of electron density. This observation is consistent with the molecule's symmetrical structure and the presence of conjugated functional groups, in particular the benzimidazole rings and the central oxadiazole unit, which may contribute to electron delocalization. The dominance of blue tones, associated with values close to zero, indicates that the molecule is more likely to engage in weak interactions such as π - π stacking, hydrophobic interactions or van der Waals forces, rather than highly polarized bonds.

The calculated energy gap ($\Delta E = 4.37$ eV) indicates a moderate electronic transition between HOMO and LUMO orbitals (**Figure 3**). This suggests that the compound has balanced reactivity and stability, making it a promising candidate for potential biological activity.

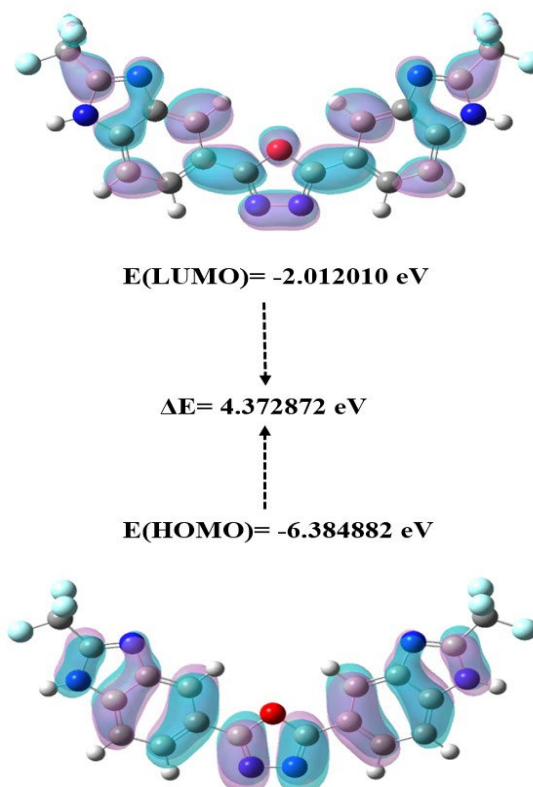


Fig. 3. HOMO and LUMO energy levels and calculated energy gap for 2,5-bis(2-(trifluoromethyl)-1H-benzo[d]imidazol-5-yl)-1,3,4-oxadiazole

3.3. ADME study and Toxicity Profil

The ADME (Absorption, Distribution, Metabolism, Excretion) properties and toxicity of the compound 2,5-bis(2-(trifluoromethyl)-1H-benzo[d]imidazol-5-yl)-1,3,4-oxadiazole were assessed using the online platform pkCSM (Pharmacokinetics and Toxicity prediction based on Graph-Based Signatures) (**Table 2 and Table 3**). These results contribute to anticipating both the pharmacokinetic performance and the toxicological profile of the compound.

Table 2. ADME prediction results of the compound 2,5-bis(2-(trifluoromethyl)-1H-benzo[d]imidazol-5-yl)-1,3,4-oxadiazole (via pkCSM).

Category	Parameter	Predicted Value (with unit)
Absorption	Water solubility (logS)	-2.89 log mol/L
	Caco-2 permeability	0.12 log Papp (10 ⁻⁶ cm/s)
	Human intestinal absorption	100 %
	Skin permeability	-2.73 log Kp
	P-glycoprotein substrate	Yes
	P-glycoprotein I inhibitor	Yes
	P-glycoprotein II inhibitor	No
Distribution	Volume of distribution (VDss)	0.13 log L/kg
	Fraction unbound (Fu)	0.29
	Blood–brain barrier (BBB) permeability	-1.76 log BB
	CNS permeability	-2.14 log PS
Metabolism	CYP2D6 substrate	No
	CYP3A4 substrate	No
	CYP1A2 inhibitor	Yes
	CYP2C19 inhibitor	Yes
	CYP2C9 inhibitor	Yes
	CYP2D6 inhibitor	No
	CYP3A4 inhibitor	Yes
Excretion	Total clearance	0.31 log mL/min/kg
	Renal OCT2 substrate	Yes

The compound exhibits low aqueous solubility (logS = -2.89), which could limit its oral bioavailability. However, human intestinal absorption is estimated at 100%, indicating excellent ability to cross the gastrointestinal barrier. Permeability across Caco-2 cells is low (log Papp = 0.12), suggesting moderate passive absorption. Regarding skin permeability, the log Kp value of -2.73 confirms low transdermal absorption. In terms of active transport, the compound is a substrate of P-glycoprotein (P-gp) and inhibits P-gp type I, but not type II, which could influence its intracellular retention and distribution.

The estimated volume of distribution (VDss) is moderate (log VDss = 0.13), indicating a moderate distribution in peripheral tissues. The free fraction in plasma is 29% (Fu = 0.29), suggesting that a significant proportion of the compound remains unbound to plasma proteins. Blood–brain barrier (BBB) permeability is low (log BB = -1.76), as is central nervous system (CNS) permeability (log PS = -2.14), indicating limited brain distribution.

The compound is not a substrate of CYP2D6 and CYP3A4, which reduces the risk of rapid metabolism via these major pathways. However, it inhibits several cytochrome isoforms: CYP1A2, CYP2C19, CYP2C9, and CYP3A4, which may lead to potential drug–drug interactions if co-administered with substrates of these enzymes.

The total clearance is moderate (log Cl = 0.31 mL/min/kg), indicating an average elimination rate. The compound is also a substrate of the renal OCT2 transporter, suggesting possible active renal excretion.

Table 3. Toxicological profile of the compound (via pkCSM).

Category	Parameter	Predicted Value (with unit)
Toxicity	AMES toxicity	Yes
	Maximum tolerated dose (human)	0.43 log mg/kg/day
	hERG I inhibitor	No
	hERG II inhibitor	Yes
	Oral rat acute toxicity (LD ₅₀)	2.46 mol/kg
	Oral rat chronic toxicity (LOAEL)	2.47 log mg/kg/day
	Hepatotoxicity	No
	Skin sensitization	No
	<i>T. pyriformis</i> toxicity	0.28 log µg/L
	Minnow toxicity	1.35 log mM

Toxicological evaluation shows the compound is positive in the Ames test, indicating mutagenic potential. The maximum tolerated dose in humans is estimated at $\log 0.43$ mg/kg/day. The compound does not inhibit hERG type I (reducing the risk of cardiac arrhythmias), but does inhibit hERG type II, which warrants further attention.

Oral acute toxicity in rats is estimated at $LD_{50} = 2.46$ mol/kg, and chronic toxicity at $LOAEL = 2.47$ log mg/kg/day. No hepatotoxic effects or skin sensitization were detected. Finally, toxicity against *Tetrahymena pyriformis* ($\log = 0.28$ $\mu\text{g/L}$) and minnow fish ($\log = 1.35$ mM) remains moderate.

3.4. Prediction of Biological Interactions via Molecular Docking

Molecular docking studies were carried out to investigate the potential therapeutic activities of 2,5-bis(2-(trifluoromethyl)-1H-benzo[d]imidazol-5-yl)-1,3,4-oxadiazole (BTBO). Docking simulations were carried out to assess the binding affinity of BTBO to various target proteins involved in key therapeutic areas, including anticancer, antibacterial, antifungal, anti-inflammatory, antioxidant and antituberculosis activities. Interaction profiles were compared to known reference ligands, with the aim of understanding how BTBO might modulate these biological pathways. Calculated affinity values and binding modes were analyzed to predict the compound's potential as a drug candidate in these therapeutic areas.

Fig. 4 and Fig. 5 illustrate the 2D (Maestro) and 3D (Discovery Studio) interaction profiles, respectively, of BTBO and Methotrexate with the active sites of the 1DLS receptor, and of the studied compounds and Ciprofloxacin with the active sites of the 4Z2D receptor.

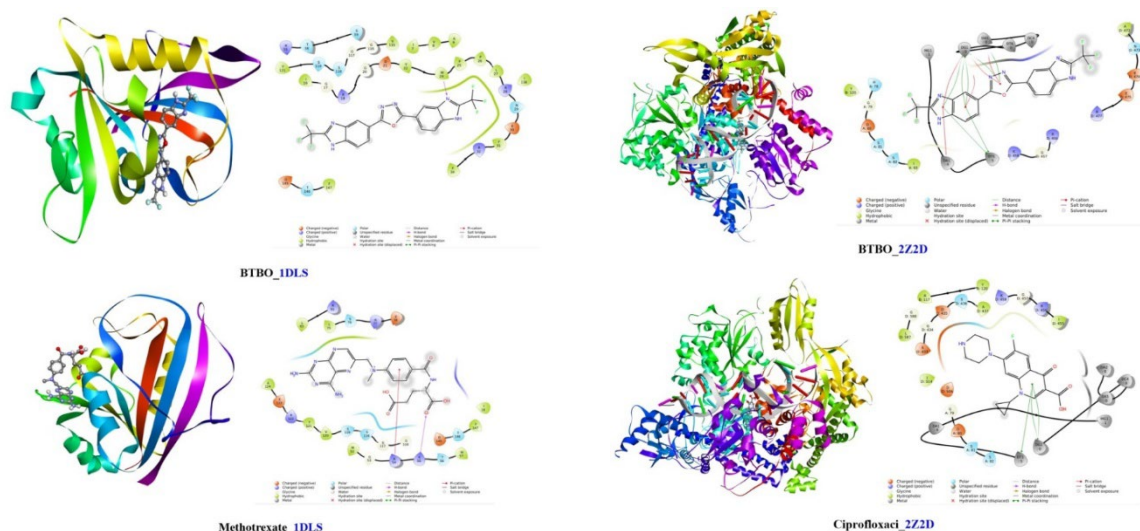


Fig. 4. 2D (Maestro) and 3D (Discovery Studio) interaction profiles of BTBO and reference ligand Methotrexate with the active sites of the 1DLS receptor

Fig. 5. 2D and 3D interaction profiles of the studied compounds and reference ligand Ciprofloxacin with the active sites of the 4Z2D receptor

Table 4 presents the binding affinities of BTBO, Methotrexate, and Ciprofloxacin with the receptors 1DLS and 4Z2D, focusing on their potential antibacterial activity. The binding affinities are given in kcal/mol, with more negative values indicating stronger binding. BTBO shows strong binding with both 1DLS (-11.8 kcal/mol) and 4Z2D (-11.6 kcal/mol), suggesting it interacts well with these receptors and has good potential for antibacterial activity. In comparison, Methotrexate binds more weakly with 1DLS at -9.1 kcal/mol, indicating that BTBO might be more effective against this receptor. Similarly, Ciprofloxacin binds with 4Z2D at -7.8 kcal/mol, which is also weaker than BTBO's binding affinity. This further suggests that BTBO could be more effective than Ciprofloxacin against this receptor. Overall, BTBO shows stronger binding to both receptors than the reference ligands, highlighting its potential as a more effective antibacterial agent

Table 4. Binding affinities (kcal/mol) of BTBO, Methotrexate, and Ciprofloxacin with 1DLS and 4Z2D receptors, highlighting the antibacterial potential of BTBO

System	Affinities (kcal/mol)
BTBO/1DLS	-11.8
Methotrexate 1DLS	-9.1
BTBO_4Z2D	-11.6
Ciprofloxaci 4Z2D	-7.8

Fig. 6 illustrates the 2D and 3D interaction profiles of BTBO and Isoniazid with the active sites of the 2H7M receptor. Table 5 presents the binding affinities of BTBO and Isoniazid with the 2H7M receptor, focusing on their potential anti-tuberculosis activity. BTBO shows strong binding with 2H7M (-10.6 kcal/mol), suggesting it interacts well with this receptor and has good potential for anti-tuberculosis activity. In comparison, Isoniazid binds weakly with 2H7M at -5.8 kcal/mol, indicating that BTBO may be more effective against this receptor. Overall, BTBO shows stronger binding to the 2H7M receptor than Isoniazid, highlighting its potential as a more effective anti-tuberculosis agent.

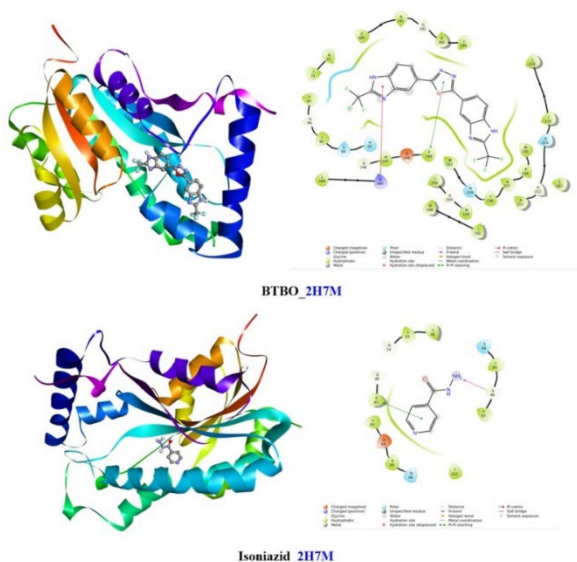


Fig. 6. 2D and 3D interaction profiles of the studied compounds and reference ligand Isoniazid with the active sites of the 2H7M receptor

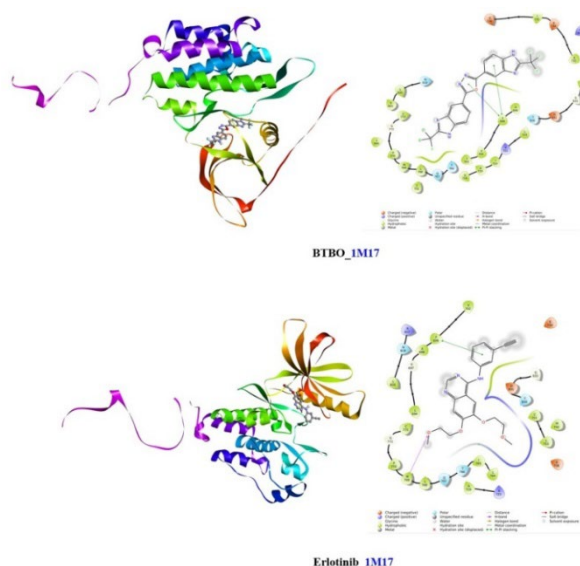


Fig 7. 2D and 3D interaction profiles of the studied compounds and reference ligand Erlotinib with the active sites of the 1M17 receptor

Table 5. Binding affinities (kcal/mol) of BTBO and Isoniazid with the 2H7M receptor, highlighting the potential anti-tuberculosis activity

System	Affinities (kcal/mol)
BTBO/2H7M	-10.6
Isoniazid 2H7M	-5.8

Figures 7 and 8 illustrate the 2D and 3D interaction profiles, respectively, of BTBO and Erlotinib with the active sites of the 1M17 receptor, and of BTBO and Venetoclax with the active sites of the 4MAN receptor.

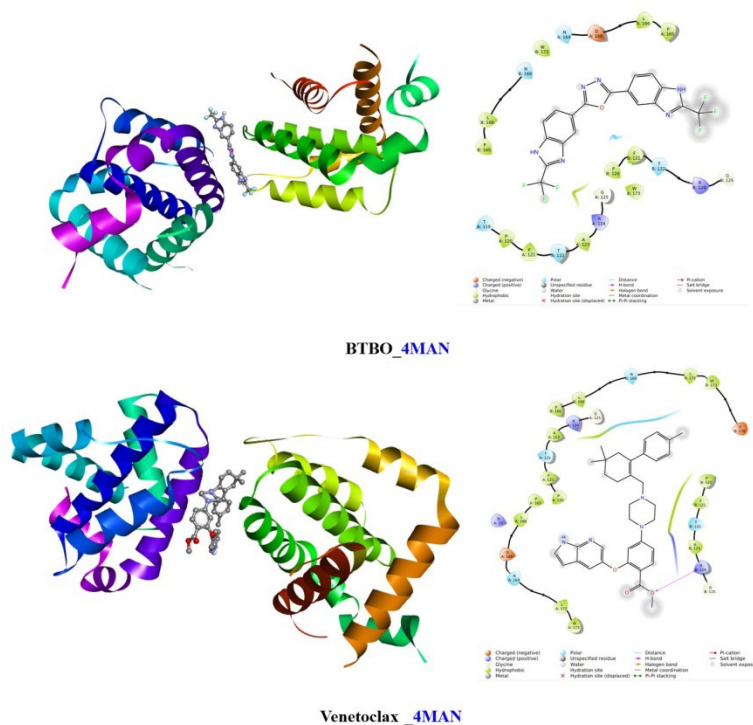


Fig 8. 2D and 3D interaction profiles of the studied compounds and reference ligand Venetoclax with the active sites of the 4MAN receptor

Table 6 shows the binding affinities (in kcal/mol) of **BTBO**, **Erlotinib**, and **Venetoclax** with the **1M17** and **4MAN** receptors, with a focus on their potential anticancer activity. Stronger binding is indicated by more negative values. **BTBO** demonstrates robust binding to both **1M17** (-9.8 kcal/mol) and **4MAN** (-9.0 kcal/mol), suggesting that it interacts effectively with these receptors and could be a promising anticancer agent. In contrast, **Erlotinib** shows weaker binding to **1M17** at -7.4 kcal/mol, suggesting that **BTBO** might be more effective against this receptor. Similarly, **Venetoclax** binds with **4MAN** at -8.9 kcal/mol, slightly less strongly than **BTBO**, further supporting the idea that **BTBO** could be more potent than the reference ligands. Overall, **BTBO** exhibits stronger binding to both receptors compared to **Erlotinib** and **Venetoclax**, reinforcing its potential as a more effective anticancer agent.

Table 6. Binding affinities (kcal/mol) of BTBO, Erlotinib, and Venetoclax with the 1M17 and 4MAN receptors, highlighting the potential anticancer activity of BTBO

Figure 9 shows the 2D and 3D **Fluconazole** with the active sites of the binding affinities of **BTBO** and receptor, focusing on their potential values of binding affinities indicate demonstrates strong binding with **5TZ1** (-11.2 kcal/mol), indicating a favorable interaction and strong potential for antifungal activity. On the other hand, **Fluconazole** binds more weakly to **5TZ1** with an affinity of -7.3 kcal/mol, suggesting that **BTBO** might be more effective for targeting this receptor. These results suggest that **BTBO** has superior binding to the **5TZ1** receptor compared to **Fluconazole**, emphasizing its potential as a more powerful antifungal agent

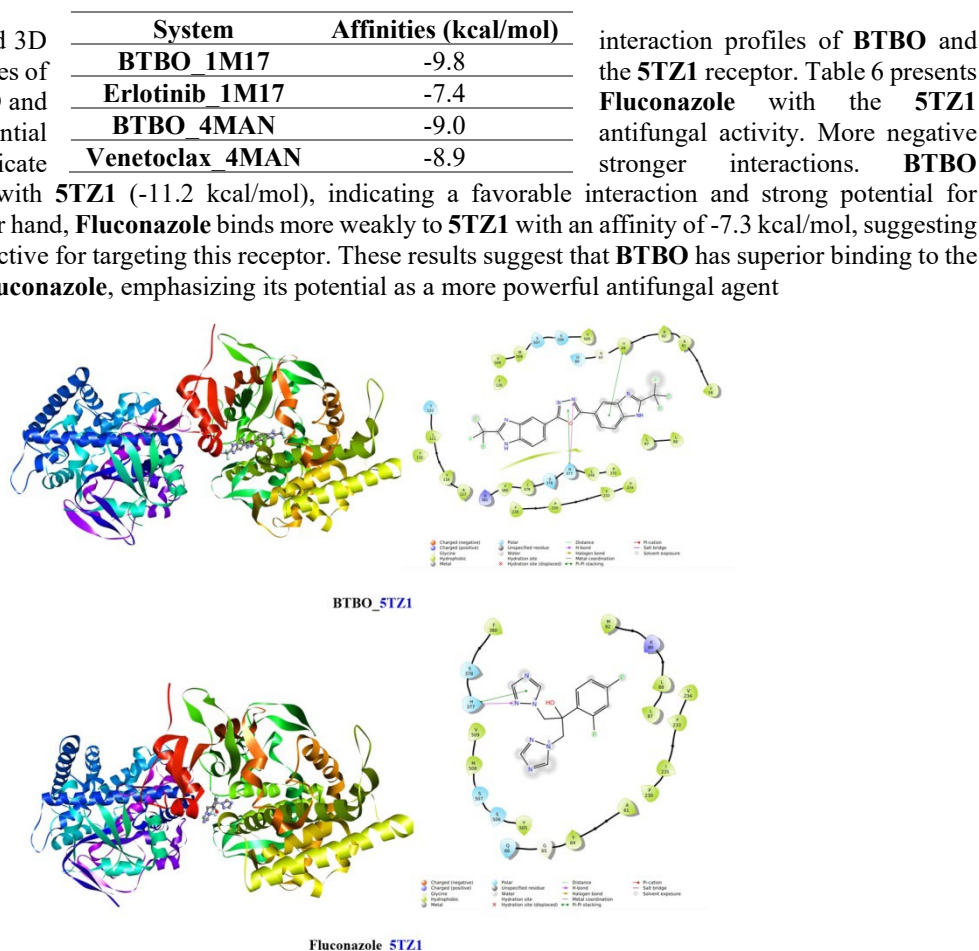


Fig 9. 2D and 3D interaction profiles of the studied compounds and reference ligand Fluconazole with the active sites of the 5TZ1 receptor

Table 7. Binding affinities (kcal/mol) of BTBO and Fluconazole with the 5TZ1 receptor, highlighting the potential antifungal activity.

System	Affinities (kcal/mol)
BTBO 5TZ1	-11.2
Fluconazole 5TZ1	-7.3

Fig. 10 illustrates the 2D and 3D interaction profiles of BTBO and Celecoxib with the active sites of the 3NT1 receptor. Table 8 presents the binding affinities of BTBO and Celecoxib with the 3NT1 receptor, focusing on their potential anti-inflammatory activity. The binding affinities are given in kcal/mol, with more negative values indicating stronger binding. BTBO shows strong binding with 3NT1 (-11.7 kcal/mol), suggesting it interacts effectively with this receptor and has good potential for anti-inflammatory activity. In comparison, Celecoxib binds more weakly with 3NT1 at -8.8 kcal/mol,

indicating that BTBO may be more effective against this receptor. Overall, BTBO exhibits stronger binding to the 3NT1 receptor than Celecoxib, highlighting its potential as a more effective anti-inflammatory agent.

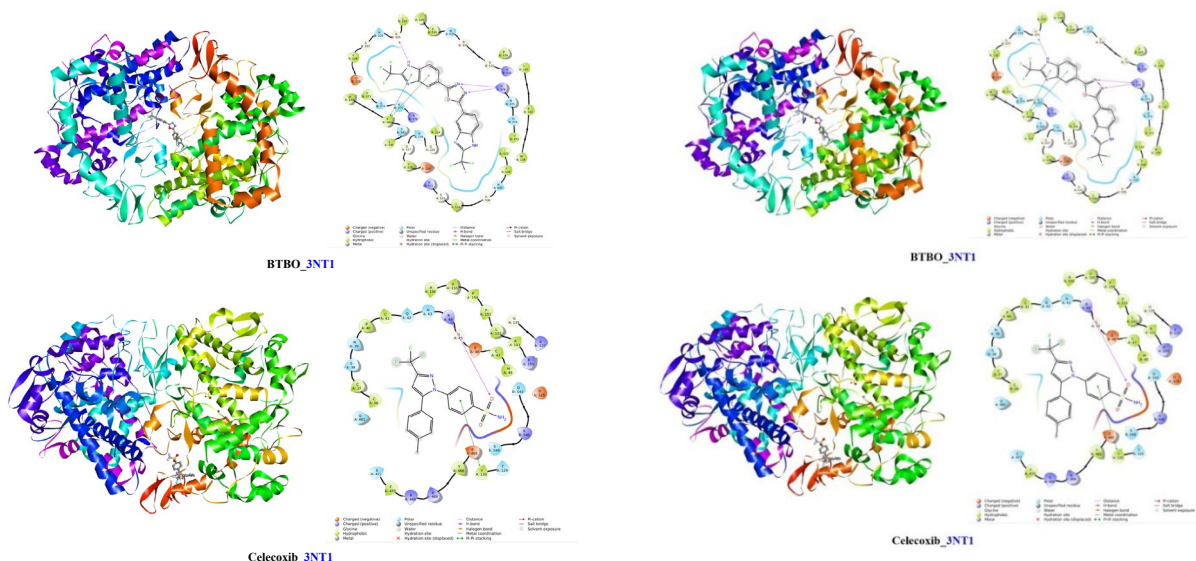


Fig. 10. 2D and 3D interaction profiles of the studied compounds and reference ligand Celecoxib with the active sites of the 3NT1 receptor

Fig 11. 2D and 3D interaction profiles of the studied compounds and reference ligand Tacrine with the active sites of the 1EVE receptor

Table 8. Binding affinities (kcal/mol) of BTBO and Celecoxib with the 3NT1 receptor, highlighting the potential anti-inflammatory activity

System	Affinities (kcal/mol)
BTBO_3NT1	-11.7
Celecoxib_3NT1	-8.8

Fig. 11 shows the 2D and 3D interaction profiles of **BTBO** and **Tacrine** with the active sites of the **1EVE** receptor. **Table 9** presents the binding affinities of **BTBO** and **Tacrine** with the **1EVE** receptor, focusing on their potential antioxidant and neuroprotective activities. The binding affinities are given in kcal/mol, with more negative values indicating stronger binding. **BTBO** shows strong binding with **1EVE** (-11.7 kcal/mol), suggesting it interacts well with this receptor and has good potential for antioxidant and neuroprotective activity. In comparison, **Tacrine** binds more weakly with **1EVE** at -8.4 kcal/mol, indicating that **BTBO** may be more effective against this receptor. Overall, **BTBO** demonstrates stronger binding to the **1EVE** receptor than **Tacrine**, highlighting its potential as a more effective antioxidant and neuroprotective agent.

Table 9. Binding affinities (kcal/mol) of BTBO and Tacrine with the 1EVE receptor, n highlighting the potential antioxidant and neuroprotective activity of BTBO.

System	Affinities (kcal/mol)
BTBO_1EVE	-11.7
Tacrine_1EVE	-8.4

4. Conclusion

This study confirms the structure of a novel 1,3,4-oxadiazole derivative, 2,5-bis(2-(trifluoromethyl)-1H-benzimidazol-5-yl)-1,3,4-oxadiazole, by ^1H NMR, ^{13}C NMR, mass spectrometry and FTIR-ATR infrared spectroscopy. Theoretical investigations provided complementary insights into its electronic reactivity and predicted promising pharmacokinetic properties, involving excellent intestinal absorption and moderate systemic distribution. Toxicological calculations revealed mutagenic potential but no hepatotoxicity or skin sensitization. Molecular docking studies highlighted strong and selective binding affinities toward various therapeutic targets, suggesting BTBO's potential as a multi-target drug candidate. Together, these findings support its promise in drug development and justify further experimental validation.

Statements & Declarations

Funding

The authors declare that no funds, grants, or other support were received during the preparation of this manuscript.

Competing Interests

The authors have no relevant financial or non-financial interests to disclose.

Acknowledgements

The authors are grateful for the research assistance from Bioorganic Chemistry Team, Faculty of Sciences, Chouaib Doukkali University, B.P. 20, 24000 El Jadida, Morocco and Molecular Modeling and Spectroscopy Research Team, Faculty of Science, Chouaib Doukkali University, P.O. Box 20, 24000 El Jadida, Morocco.

References

1. Varala R., Kurra M., Amanullah M., Hussien M., and Alam M. M. (2024) Recent methods in the synthesis of chromeno [2, 3-d] pyrimidines. *Chem. Heterocycl. Compd.*, 60(3) 111-117.
2. Pace A., and Pierro P. (2009) The new era of 1, 2, 4-oxadiazoles. *Org. Biomol. Chem.*, 7(21) 4337-4348.
3. Boström J., Hogner A., Llinàs A., Wellner E., and Plowright, A. T. (2012) Oxadiazoles in medicinal chemistry. *J. Med. Chem.*, 55(5) 1817-1830.
4. Delaugerre C. (2010) Genetic barrier to antiretroviral drug-resistance. Focus on raltegravir, the first integrase inhibitor. *MMI Formation*, 4(1) 1-10.
5. Sultana R., Ali A., Rana M., Ahmad I., Kamthan M., Almuqdad H. T. A., Mehandi R., Abid M., and El-Bahy Z. M. (2024) Synthesis of oxadiazole derivatives: Anti-bacterial, DNA binding and in silico molecular modelling approaches. *J. Mol. Struct.*, 131(2) 139350.
6. James N. D., and Growcott J. W. (2009) Zibotentan. *Drugs Future.*, 34(8) 624-633.
7. Banerjee A. G., Das N., Shengule S. A., Srivastava R. S., and Shrivastava S. K. (2015) Synthesis, characterization, evaluation and molecular dynamics studies of 5, 6-diphenyl-1, 2, 4-triazin-3 (2H)-one derivatives bearing 5-substituted 1, 3, 4-oxadiazole as potential anti-inflammatory and analgesic agents. *Eur. J. Med. Chem.*, 101(2015) 81-95.
8. Gulnaz A. R., Mohammed Y. H. E., and Khanum S. A. (2019) Design, synthesis and molecular docking of benzophenone conjugated with oxadiazole sulphur bridge pyrazole pharmacophores as anti-inflammatory and analgesic agents. *Bioorg. Chem.*, 92(2019) 103220.
9. Abd-Ellah H. S., Abdel-Aziz M., Shoman M. E., Beshr E. A., Kaoud T., and Ahmed A. S. F. (2017) New 1, 3, 4-oxadiazole/oxime hybrids: Design, synthesis, anti-inflammatory, COX inhibitory activities and ulcerogenic liability. *Bioorg. Chem.*, 74(2017) 15-29.
10. Jayashankar B., Rai K. L., Baskaran N., and Sathish H. S. (2009) Synthesis and pharmacological evaluation of 1, 3, 4-oxadiazole bearing bis (heterocycle) derivatives as anti-inflammatory and analgesic agents. *Eur. J. Med. Chem.*, 44(10) 3898-3902.
11. Kaur J., Soto-Velasquez M., Ding Z., Ghanbarpour A., Lill M. A., van Rijn R. M., Watts V, J., and Flaherty D. P. (2019) Optimization of a 1, 3, 4-oxadiazole series for inhibition of Ca²⁺/calmodulin-stimulated activity of adenylyl cyclases 1 and 8 for the treatment of chronic pain. *Eur. J. Med. Chem.*, 162(2019) 568-585.
12. Tantray M. A., Khan I., Hamid H., Alam M. S., Dhulap A., and Kalam A. (2018) Synthesis of benzimidazole-linked-1, 3, 4-oxadiazole carboxamides as GSK-3 β inhibitors with in vivo antidepressant activity. *Bioorg. Chem.*, 77(2018) 393-401.
13. Singh P., Sharma P. K., Sharma J. K., Upadhyay A., and Kumar N. (2012) Synthesis and evaluation of substituted diphenyl-1, 3, 4-oxadiazole derivatives for central nervous system depressant activity. *Bioorg. Med. Chem. Lett.*, 2(8) 1-10.
14. Yadagiri B., Gurralla S., Bantu R., Nagarapu L., Polepalli S., Srujana G., and Jain N. (2015) Synthesis and evaluation of benzosuberone embedded with 1, 3, 4-oxadiazole, 1, 3, 4-thiadiazole and 1, 2, 4-triazole moieties as new potential anti proliferative agents. *Bioorg. Med. Chem. Lett.*, 25(10) 2220-2224.
15. Glomb T., Szymankiewicz K., and Świątek P. (2018) Anti-cancer activity of derivatives of 1, 3, 4-oxadiazole. *mol.*, 23(12) 3361.
16. Shyma P. C., Balakrishna K., Peethambar K. S., and Vijesh M. A. (2015) Synthesis, characterization, antidiabetic and antioxidant activity of 1, 3, 4-oxadiazole derivatives bearing 6-methyl pyridine moiety. *Der Pharma Chem*, 7(12) 137-45.
17. Nazreen S., Alam M. S., Hamid H., Yar M. S., Shafi S., Dhulap A., Alam P., Pasha M. A. Q., Bano S., Alam M. M., Haider S., Ali Y., Kharbanda C., and Pillai K. K. (2014) Design, synthesis, in silico molecular docking and biological evaluation of novel oxadiazole based thiazolidine-2, 4-diones bis-heterocycles as PPAR- γ agonists. *Eur. J. Med. Chem.*, 87(2014) 175-185.
18. Şahin G., Palaska E., Ekizoğlu M., and Özalp M. (2002) Synthesis and antimicrobial activity of some 1, 3, 4-oxadiazole derivatives. *Il Farmaco*, 57(7) 539-542.
19. Ali M. A., and Shaharyar M. (2007) Oxadiazole mannich bases: Synthesis and antimycobacterial activity. *Bioorg. Med. Chem. Lett.*, 17(12) 3314-3316.

20. Rane R. A., Bangalore P., Borhade S. D., and Khandare P. K. (2013) Synthesis and evaluation of novel 4-nitropyrrole-based 1, 3, 4-oxadiazole derivatives as antimicrobial and anti-tubercular agents. *Eur. J. Med. Chem.*, 70(2013) 49-58.
21. Zoumpoulakis P., Camoutsis C., Pairas G., Soković M., Glamočlija J., Potamitis C., and Pitsas A. (2012) Synthesis of novel sulfonamide-1, 2, 4-triazoles, 1, 3, 4-thiadiazoles and 1, 3, 4-oxadiazoles, as potential antibacterial and antifungal agents. Biological evaluation and conformational analysis studies. *Bioorg. Med. Chem.*, 20(4) 1569-1583.
22. Xu W., He J., He M., Han F., Chen X., Pan Z., Wang X and Tong, M. (2011). Synthesis and antifungal activity of novel sulfone derivatives containing 1, 3, 4-oxadiazole moieties. *mol.*, 16(11) 9129-9141.
23. Johns B. A., Weatherhead J. G., Allen S. H., Thompson J. B., Garvey E. P., Foster S. A., Jeffrey J. L., and Miller W. H. (2009) 1, 3, 4-Oxadiazole substituted naphthyridines as HIV-1 integrase inhibitors. Part 2: SAR of the C5 position. *Bioorg. Med. Chem. Lett.*, 19(6) 1807-1810.
24. El-Sayed W. A., El-Essawy F. A., Ali O. M., Nasr B. S., Abdalla M. M., and Abdel-Rahman A. A. H. (2009) Anti-HIV activity of new substituted 1, 3, 4-oxadiazole derivatives and their acyclic nucleoside analogues. *Z. Naturforsch. C*, 64(11-12) 773-778.
25. Hanson M. D. (2024) Visualizing the Hydrogen Atomic Orbitals: A Tool for Undergraduate Physical Chemistry. *J. Chem. Educ.*, 101(8) 3539-3546
26. Gokcan H., and Isayev O. (2022) Learning molecular potentials with neural networks. *Wiley Interdiscip. Rev. Comput. Mol. Sci.*, 12(2) e1564.
27. Daina A., Michielin O., and Zoete V. (2017) SwissADME: a free web tool to evaluate pharmacokinetics, drug-likeness and medicinal chemistry friendliness of small molecules. *Sci. Rep.*, 7(1) 42717.
28. Morris G. M., Huey R., Lindstrom W., Sanner M. F., Belew R. K., Goodsell D. S., and Olson A. J. (2009) AutoDock4 and AutoDockTools4: Automated docking with selective receptor flexibility. *J. Comput. Chem.*, 30(16) 2785-2791.
29. Kerraj S., Al-Zaydi K. M., Moussaoui M., Salah, M., and Belaouad S. (2024) Functionalized η 6-Arene Chromium Half-Sandwich Complexes in DSSC Performance: A Theoretical Perspective. *Sci. Afr.*
30. Sliwoski G., Kothiwale S., Meiler J., and Lowe Jr, E. W. (2014) Computational methods in drug discovery. *Pharmacol. Rev.*, 66(1) 334-395.
31. Trott O., and Olson A. J. (2010) AutoDock Vina: improving the speed and accuracy of docking with a new scoring function, efficient optimization, and multithreading. *J. Comput. Chem.*, 31(2) 455-461.
32. Dhannur S. H., Shridhar A. H., Suresh S., Al-Asbahi B. A., Al-Hada N. M., Shelar V. M., and Naik, L. (2024) DFT studies on D-π-A substituted bis-1, 3, 4-oxadiazole for nonlinear optical application. *J. Opt.*, 53(5) 5079-5089.
33. Yurovskaya M. A., and Afanas' ev A. Z. (1991) Methods for the synthesis of 3-nitropyridines. *Chem. Heterocycl. Compd.*, 27(7) 681-707.
34. Sadowski M., and Kula K. (2024) Unexpected course of reaction between (1E,3E)-1,4-Dinitro-1,3-butadiene and n-methyl azomethine ylide—a comprehensive experimental and quantum-chemical study. *molecules.*, 29(21) 5066.
35. « Protein Data Bank | Nucleic Acids Research | Oxford Academic ». Consulté le: 22 avril 2025. [En ligne]. Disponible sur: <https://academic.oup.com/nar/article/28/1/235/2384399>
36. Kim S., Chen J., Cheng T., Gindulyte A., He J., He S., Li Q., Shoemaker A. B., Thiessen A. P., Yu B., Zaslavsky L., Zhang J., and Bolton, E. E. (2021) PubChem in 2021: new data content and improved web interfaces. *Nucleic. Acids. Res.*, 49(D1) D1388-D1395.
37. Navarrete-Vázquez G., Cedillo R., Hernández-Campos A., Yépez L., Hernández-Luis F., Valdez J., Morales R., Cortes R., Hernandez M., and Castillo R. (2001) Synthesis and antiparasitic activity of 2-(trifluoromethyl) benzimidazole derivatives. *Bioorg. Med. Chem. Lett.*, 11(2) 187-190.
38. Al-Zobaydi S. F., Karim B., Al-Sahib S. A., and Ismael B. D. (2016) Synthesis, Characterization of some New 1, 3, 4-Oxadiazole derivatives based on 4-amino benzoic acid. *Baghdad Sci. J.*, 13(2.2 NCC) 0289-0289.
39. Luiksaar S. I., Belen'kii L. I., and Krayushkin M. M. (1998) An efficient synthesis of symmetrical 2, 5-diaryl-1, 3, 4-oxadiazoles. *Mendeleev Commun.*, 8(4) 136-137.
40. Al-Zobaydi S. F., Karim B., Al-Sahib S. A., and Ismael B. D. (2016) Synthesis, Characterization of some New 1, 3, 4-Oxadiazole derivatives based on 4-amino benzoic acid. *Baghdad Sci. J.*, 13(2.2 NCC) 0289-0289.
41. Hendrickson J. B., and Hussoin M. S. (1989) Reactions of carboxylic acids with phosphonium anhydrides. *J. Org. Chem.*, 54(5) 1144-1149.
42. Kaul S., Kumar A., Sain B., and Bhatnagar A. K. (2007) Simple and convenient one-pot synthesis of benzimidazoles and benzoxazoles using N, N-Dimethylchlorosulfitemethaniminium chloride as condensing agent. *Synth. Commun.*, 37(15) 2457-2460.
43. Phillips M. A. (1928) CCCXVII.—The formation of 2-substituted benzimidazoles. *J. Chem. Soc.*, 0, 2393-2399.
44. MoloU K. Y., and SISSoUMa D. (2010) Synthèse de 2-hétéroarylbenzimidazoles à visée anti-infectieuse par application de la réaction de phillips. *J. sci*, 11(2) 40-51.

